Transfer of Graded Potentials at the Photoreceptor-Interneuron Synapse

M. JUUSOLA, R. O. UUSITALO, and M. WECKSTRÖM

From the Department of Physiology, University of Oulu, Kajaanintie 52 A 90220 Oulu, Finland

ABSTRACT To characterize the transfer of graded potentials and the properties of the associated noise in the photoreceptor-interneuron synapse of the blowfly (*Calliphora vicina*) compound eye, we recorded voltage responses of photoreceptors (R1–6) and large monopolar cells (LMC) evoked by: (*a*) steps of light presented in the dark; (*b*) contrast steps; and (*c*) pseudorandomly modulated contrast stimuli at backgrounds covering 6 log intensity units. Additionally, we made recordings from photoreceptor axon terminals. Increased light adaptation gradually changed the synaptic signal transfer from low-pass to band-pass filtering. This was accompanied by decreased synaptic delay and increased contrast gain, but the overall synaptic gain and the intrinsic noise (i.e., transmission noise) were reduced. Based on these results, we describe a descriptive synaptic model, in which the kinetics of the tonic transmitter (histamine) release from the photoreceptor axon terminals change with mean photoreceptor depolarization. During signal transmission, tonic transmitter release is augmented by voltage-dependent contrast-enhancing mechanisms in the photoreceptor axons that produce fast transients from the rising phases of the photoreceptor responses and add these enhanced voltages to the original photoreceptor responses. The model can predict the experimental findings and it agrees with the recently proposed theory of maximizing sensory information.

INTRODUCTION

Adaptation allows sensory systems to regulate their sensitivity to changes in the environmental stimulus energy (reviewed by Koshland, Goldbeter, and Stock, 1982; Shapley and Enroth-Cugell, 1984; Laughlin, 1989). To maximize information gathering and to minimize the effects of the accompanying noise, the processing of sensory signals requires that adaptive mechanisms operate, not only in sensory cells, but also at other levels of sensory systems. In the blowfly compound eye, the dynamic visual images sampled by the photoreceptors are synaptically transmitted to the large monopolar cells (LMCs) in the form of graded potentials, and this process includes synaptic adaptation (Autrum, Zetler, and Järvilehto, 1970; Järvilehto and Zettler, 1971, 1973; Zettler and Järvilehto, 1971, 1972; Laughlin and Hardie, 1978; Laughlin, Howard, and Blakeslee, 1987). Axons of six (R1–6) photoreceptors from six different ommatidia, all receiving information about light intensity from the same

Address correspondence to Dr. Mikko Juusola, Department of Physiology, University of Oulu, Kajaanintie 52 A 90220 Oulu, Finland.

J. GEN. PHYSIOL. © The Rockefeller University Press · 0022-1295/95/01/0117/32 $2.00 117
Volume 105 January 1995 117–148

spatial angle, converge on the first visual ganglion (*Lamina ganglionaris*), presumably to improve the postsynaptic signal-to-noise ratio (SNR) (Kirschfeld, 1967; Strausfeld, 1971; Dubs, Laughlin, and Srinivasan, 1981; van Hateren, 1986, 1993; Laughlin et al., 1987). In the lamina, the image is modified before transmission to the next visual ganglion, the medulla: the photoreceptor signals are encoded into postsynaptic LMC responses by amplification, transient generation (phasic on- and off-responses) and filtering, the strength of which depends on ambient light (Järvilehto and Zettler, 1971; Laughlin et al., 1987). Most of these changes have been suggested to occur presynaptically—at a cost of low frequencies—allowing rapid transmission of signals across the synapse (Laughlin and Osorio, 1989; Weckström, Juusola, and Laughlin, 1992*a*).

When a fly is moving, temporal and spatial changes in the reflectance of objects cause fluctuating voltage responses in the photoreceptors and LMCs (Laughlin, 1981*a;* Howard, Blakeslee, and Laughlin, 1987; Juusola, Kouvalainen, Järvilehto, and Weckström, 1994). Although the light intensity levels in the environment can vary by as much as 10^9-fold in the day time, the relative contrast remains unchanged between different objects (Laughlin, 1987). To provide the maximum sensitivity for detecting light contrast, photoreceptors and LMCs adjust their operations according to the mean light intensity level, i.e. the adapting background (Laughlin and Hardie, 1978; Laughlin, 1987; Laughlin et al., 1987; Juusola, 1993; Juusola et al., 1994). To maximize the SNR for the transmitted band of frequencies, and to fully occupy the limited information capacity of the channel (cf. van Hateren, 1992*a,b,c,* 1993) the visual signal undergoes adaptive filtering.

We have studied how adaptational changes in early visual processing influence the temporal properties of transmitted signals by a combination of both the time and frequency domain analysis. To obtain virtually noise-free conditions, a pseudorandomly modulated light stimulation in conjunction with time-domain averaging was the method of choice. We made reliable estimates of the synaptic transfer characteristics and of the linearity of the system. In addition, the effects of noise were separated from the properties of the synapse itself. Our results lead to a descriptive model of signal transfer in the synapse, based on a combination of tonic transmitter release, that changes its kinetics with the mean photoreceptor potential, and axonally enhanced photoreceptor responses.

MATERIALS AND METHODS

Principles of the Approach

The main objective was to characterize synaptic transmission by recording presynaptically (R1–6 photoreceptors) and postsynaptically (LMCs) during controlled light stimulation. Because of the small size of the pre- and postsynaptic cells, we could not get simultaneous recordings from them. To characterize the signal processing properties of a photoreceptor or an LMC at a certain illumination, reproducible behavior had to be found from all cells of the same type under the same stimulus conditions. In this paper, we have conceptualized the synaptic interconnection as a "black box" that receives certain input signals and produces certain output signals. This method allowed us to bypass complex biophysical events at subcellular level and concentrate on the process of signal transmission. To achieve a reliable model of the synaptic signal processing, the quality of both the presynaptic and the

postsynaptic recordings had to be excellent, representing the true characteristics of the cells as well as possible, and the recording settings of the system had to be constant so that the system was fully adapted to the chosen background. A thorough description of the transfer function and noise analysis is given in the Appendix and in Fig. 16.

Animals and Preparation

We used adult blowflies (*Calliphora vicina*) of both sexes. They were cultured in our laboratory, where they were fed with sugar and yeast. The stock was refreshed frequently with wild flies.

Flies were attached with bees wax to a rotatable recording platform and grounded with an indifferent electrode (Ag/AgCl) positioned inside the head. Intracellular recordings of LMCs and R1–6 photoreceptors were performed via glass capillary microelectrodes, which were moved with a piezoelectric microtranslator (Burleigh inchworm PZ-550) into the tissues of the lamina and retina through a small hole made on the lateral cornea and sealed with a high vacuum grease. The resistance of the microelectrodes, filled with either 3 M KCl or with a mixture of 2.5 mM KCl and 1.5 M K-acetate, varied between 80 and 250 MΩ with the electrode in the tissue. All experiments were conducted at room temperature (21 ± 1°C) and were started after 30 min of dark adaptation.

Light Stimuli

The light source was an LED (Stanley HBG 5666X, with peak emission at 555 nm) mounted on a cardan arm. The LED constituted a pointlike stimulus subtending ~1.5°, thus giving negligible stimulation to the lateral inhibitory system (Laughlin, 1987). Computer aided stimulation of cells was performed by using light steps in darkness or superimposed on a steady light background (with step duration varied from 2 to 300 ms), and pseudorandomly modulated light stimuli. The LED was driven by a current source, whose output range was limited to the linear range of the current-light intensity relation. The contrast (c) of the step stimuli was defined as:

$$c = \frac{\Delta I}{I_{mean}} \tag{1}$$

where ΔI was the change in illumination and I_{mean} was the mean background. The contrast of the pseudorandom stimulus was defined analogously, except that ΔI represented the SD of the intensity modulation (Fig. 1 *A;* see Juusola, 1993; Kouvalainen, Weckström, and Juusola, 1994; Juusola et al., 1994). The pseudorandom stimulus had a Gaussian intensity distribution (Fig. 1 *B*) and the power spectrum was flat up to ~200 Hz (Fig. 1 *C*). Light was attenuated by neutral density filters (Kodak Wratten) to provide an intensity range of more than 6 log units. The response amplitudes of the cells were tested by steps. Cells were rejected if the amplitude changed during the considerably long recording procedures. To have a steady increase in light adaptation, the stimulation was performed from the weakest to the strongest adapting background. After experiments, cells were re-dark-adapted and the recordings were rejected if the cell's sensitivity did not return to the initial values.

Recording Procedures

In R1–6 photoreceptor somata recordings, the corneal negative ERG and frequent microelectrode penetrations from one photoreceptor to another indicated the correct retinal recording site. Penetration into the lamina was verified by the corneal positive ERG and by the alternating impalements of photoreceptor axons and LMCs as the electrode was advanced in tissue. The identification of LMC types was based on differences in the resting potentials and input resistances, and on the distinct shape of L3's responses, the off spike (Hardie and Weckström,

1990). However, the main point of this study was to characterize the general principles of signal transfer in the photoreceptor-LMC synapse, not to concentrate on the slight differences between the responses of the LMC-types.

When light-adapted, recording of cell responses were started only well after the on transient of a cell, arising from the initial change of light stimulation, had subsided and a steady polarization was achieved (~2 min). After this we were able to accurately control the system's

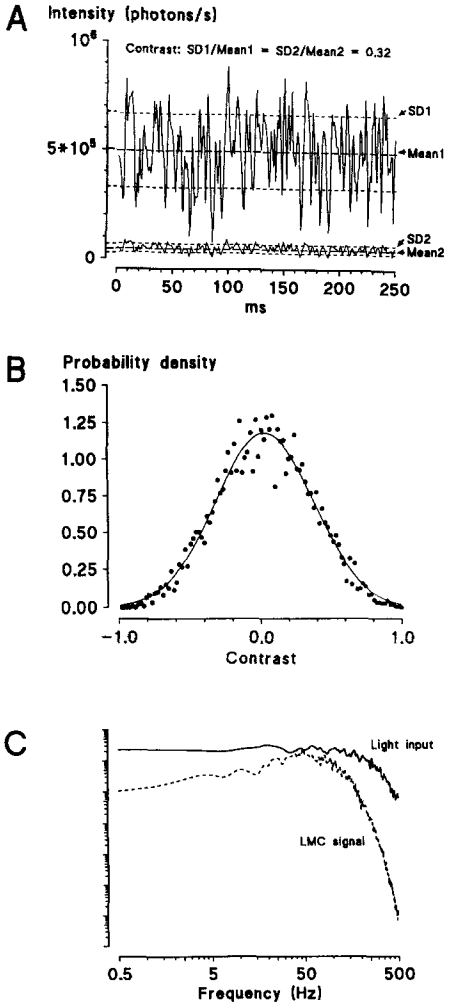

FIGURE 1. Characteristics of the pseudorandomly modulated light contrast stimulus. (*A*) 250-ms sample of the stimulus sequence with contrast of 0.32 at two mean intensity levels, i.e., adapting backgrounds. The contrast of the stimulus is defined in the text. (*B*) The probability density function of the amplitude of the pseudorandom stimulus shows the Gaussian distribution of the stimulation intensity. The solid line is k*exp $\{-[(x-u)^2]/(2*s^2)\}$; $u = 0.021$, $s = 0.333$, $k = 1.125$ and $r^2 = 0.966$. (*C*) Power spectra of the pseudorandom light input and 210-times averaged LMC responses at an adapting background of 500,000 photons/s. The input spectrum was approximately flat up to 250 Hz, well beyond the 3-dB cut-off frequency of the output power spectrum (of the LMC response). Signals were filtered at 500 Hz.

adaptational state as well as use various forms of contrast stimulation. The cell responses were transmitted via a microelectrode to a high impedance preamplifier (SEC-1L, npi Electronic, Tamm, Germany) and filtered, together with the corresponding LED stimulus current (VBF/23 low pass dual channel elliptic filter, KEMO). Both the signals were then monitored on an oscilloscope, sampled at 2 KHz, digitized with a 12-bit A/D converter (DT2821, Data Translation, Inc., Marlboro, MA) and stored on hard disk or in the memory of a computer (IBM-486 compatible with 33 MHz). The sampling process was initiated synchronously to the

contrast signals produced by the computer, and 0.5- (step stimuli) or 8-s (pseudorandom modulation) records of both signals were obtained during each recording cycle. After a preset number of responses (usually 10–100) the average response was calculated (see also French, 1980*a*,*b*).

RESULTS

We investigated the properties of signal transfer in the R1–6 photoreceptor-LMC synapse in the dark and at eight different adapting backgrounds. For this analysis we used (*a*) pre- and postsynaptic step responses to identical stimuli, (*b*) responses to pseudorandom light stimulus, (*c*) transfer functions, (*d*) noise power spectra, and (*e*) signal-to-noise ratios. Below we follow the results of this analysis in the same order, first examining adaptational changes on the dynamics of signal transfer, then considering the effects of simultaneously generated noise and finally demonstrating how these changes alter the postsynaptic signal-to-noise ratio, SNR. We also show the signal enhancement in photoreceptor axon terminals. Altogether, over 250 photoreceptors, 200 LMCs, and 20 photoreceptor axon terminals were recorded from. The transfer functions and the noise data were calculated from 30 LMCs, 40 photoreceptors and from three photoreceptor axon terminals. For transfer function determinations we used only cells with the best possible recording stability. It was found that stable photoreceptor impalements yielding a maximum dark-adapted response of ~60 mV and input resistance of larger than 30 MΩ always resulted in a nearly equal frequency response (cf. Juusola et al., 1994). The same finding applies to stable LMC recordings, with large (>40 mV) dark-adapted response and >15 MΩ input resistance. The cell to cell variability had thus a negligible effect on the analysis (for confidence intervals, see Appendix).

Step Responses

The photoreceptor and LMC responses were first studied after 30 min of dark-adaptation with light steps. Only cells with adequate response amplitudes and recording stability were chosen for further experiments. Figs. 2 and 3 compare the step responses of a photoreceptor to those of a LMC in darkness and at an adapting background of ~500,000 photons/s.

Dark-adapted cells. Photoreceptors responded to light steps of exponentially increasing intensity with characteristic graded depolarizations that saturated between 55 and 70 mV before gradually attenuating towards the plateau potentials set by the illumination (Figs. 2*A* and 3*A*). The adaptational decay of the larger responses demonstrated a damped oscillation, or a dip, ~50 ms from the initiation of the light step. The magnitude of the dip depended on the interstimulus period (data not shown), thus, the shorter was this duration, the smaller was the dip, vanishing totally with periods <200 ms. In LMCs the resulting postsynaptic graded potentials were substantially modified. Fig. 2*B* shows how an LMC (here L3; identified by its low dark resting potential and by the characteristic off spike; see Hardie and Weckström, 1990) responded to changes in retinal illumination with transient on-off-phasic polarizations that were inverted from those of photoreceptor responses. The on-transients of the LMCs were saturated even with small 2-ms light steps of 200 photons/s, which hyperpolarized LMC responses 40–58 mV below the dark resting

potential (Fig. 3 *A*). In general, LMC responses had substantially more rapid time courses than the photoreceptors; their rising phase was considerably steeper and as a result they reached peak responses in a shorter period of time when calculated form the light onset (cf. Järvilehto and Zettler, 1971). Further, the slowly decaying potentials of the photoreceptors during 300-ms steps were far less obvious in LMC responses, whereas the dip in photoreceptors seemed to correspond temporally with a depolarizing oscillation in LMCs (as seen in Fig. 2 *B*).

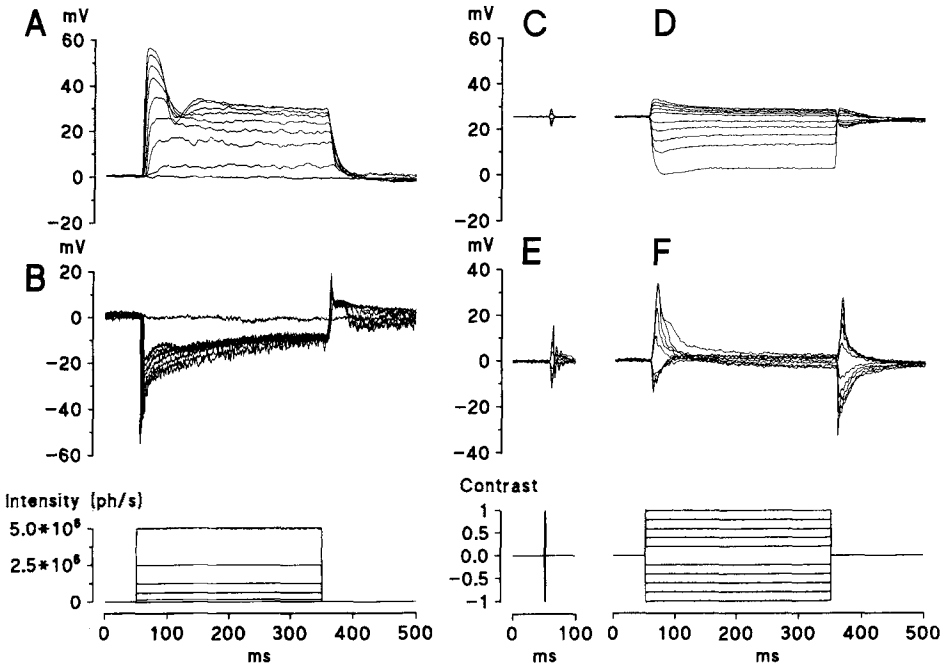

FIGURE 2. Intracellular recordings from a R1–6 photoreceptor and a LMC. Voltage responses of a dark adapted photoreceptor (*A*) and an LMC (*B*) to 300-ms light steps with a step interval of 1.5 s, no averaging. Note the dip in the responses during the strongest illumination. Voltage responses of a light adapted photoreceptor (*C*) and an LMC (*E*) to 2-ms contrast steps, and to 300-ms contrast steps (*D* and *F*), respectively. The adapting background was ~500,000 photons/s with a step interval of 0.4 s, contrast from −1.00 to 1.12. The contrast responses were averaged 10 times. Zero on the voltage scale represents the dark resting potential of the cell.

Light-adapted cells. The amplitudes of the photoreceptor responses in light-adapted cells were much reduced compared to dark-adapted cells. With the background of 500,000 photons/s, the contrast responses were superimposed on a mean depolarization of ~20 mV above the dark resting potential. Fig. 3 *B* shows a characteristic relationship between different contrast steps and the peak amplitudes of the photoreceptor responses seen in Fig. 2, *C* and *D*. As reported earlier by Juusola (1993), regardless of the background intensity, brief contrast steps elicited approximately linear photoreceptor responses. Moreover, as the contrast duration

was increased, the hyperpolarizing responses increased more than the corresponding depolarizing ones. Such nonlinear behavior results from a response compression that increases the illumination range over which photoreceptors can operate with a good SNR (see also Juusola et al., in press; French, Korenberg, Järvilehto, Kouvalainen, Juusola, and Weckström, 1993). Contrary to photoreceptors, LMCs adapted to the

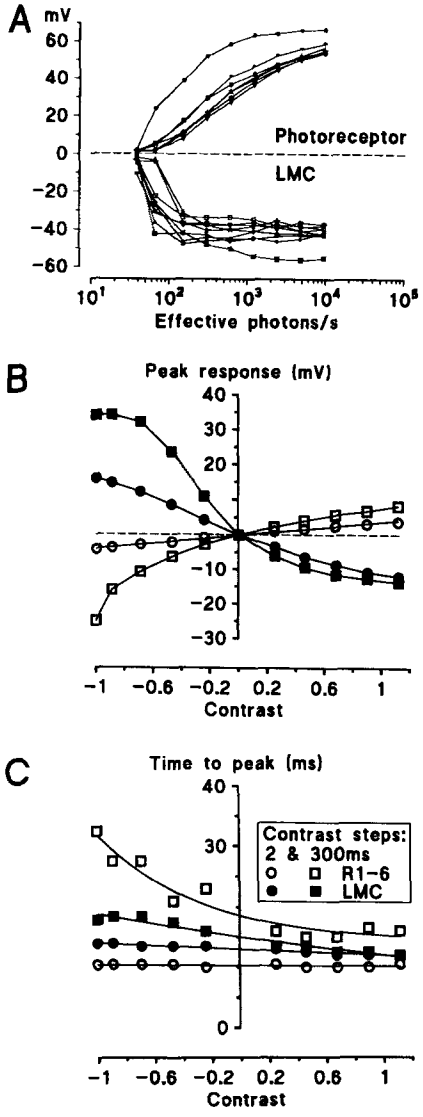

FIGURE 3. Peak parameters of photoreceptor and LMC responses with a 300-ms stimulus. (*A*) Peak-response values of dark-adapted cells (eight photoreceptors and nine LMCs) to different light step intensities. Note how the LMC responses saturate at much lower intensities than the photoreceptors. (*B* and *C*) 20-times averaged peak-response amplitudes and the corresponding time-to-peak values of the light-adapted photoreceptor and the LMC shown in Fig. 2 (*C–F*). The values are represented as a function of contrast.

change in background, i.e., contrast stimulus, within 300 ms, as their membrane potential approached the dark-adapted values (Fig. 2 *F*). The response dynamics in individual LMC recordings were similar with transient on and off transients, but there was a fairly large variation in the peak amplitudes under identical stimulation,

apparently not connected with recording quality. For example, the maximum on transients varied from cell to cell between 7 and 22 mV. However, the size of on transients in individual cells increased only negligibly, as the step duration was increased from 2 to 300 ms (Figs. 2, *E* and *F*, and 3 *B*). This suggested that the size of the postsynaptic on transients could be related to the fastest changes in the photoreceptor responses. The time course of the postsynaptic responses at a given background were independent of the step duration, yet directly proportional to the value of contrast used, as in photoreceptors with short (1–2 ms) contrast steps (cf. Howard et al., 1987; Laughlin et al., 1987; Juusola, 1993). How do these findings correlate with time-to-peak values?

With 300-ms contrast steps, the LMC responses were significantly faster than the corresponding photoreceptor responses. Judging from the examples (Figs. 2, *E* and *F*), LMC responses lead photoreceptor responses by 5 ms with a contrast of +1 and by 15 ms with a contrast of −1 (Fig. 3 *C*). This superficially noncausal time course indicates that during long contrast steps, the presynaptic peak amplitudes cannot themselves be responsible for the maximum amplitudes of the postsynaptic responses. At this point, one might contemplate calculating the peak-voltage transfer of the photoreceptor-LMC synapse in the light-adapted state by comparing the corresponding photoreceptor response amplitudes elicited by long contrast steps to the postsynaptic ones at the time of LMC peak responses. Unfortunately, such a method would be inaccurate, because it completely disregards the changing delays and the synaptic transfer function that modify the light adaptational dynamics of the signal transfer. In addition, the synapse appears to function very nonlinearly with steplike stimuli, but fairly linearly with noise stimulus more closely mimicking natural conditions. It will be shown below that both the transfer delay and the synaptic transfer functions vary in a time- and adaptation-dependent manner. Therefore, using any fixed values for them would yield biased estimates of the synaptic gain.

As shown in Fig. 3, the time course of the LMC on-transients stayed fairly constant as the contrast step duration was increased from 2 to 300 ms. Moreover, these responses were nearly as fast as the photoreceptor responses to 2 ms contrast steps. Thus, varying from one experiment to another and again without obvious connection to impalement quality, the peaks of photoreceptor responses led the peaks of LMC responses by 0.5–3.5 ms under the same illumination. The variations in the delay depended almost entirely on the cells. LMCs that had larger peak responses were generally slower than those with smaller peak-responses. However, regardless of these differences, the causal order of pre- and postsynaptic impulse responses (elicited by 1- and 2-ms contrast steps) (Fig. 3 *B*) allowed us to estimate the synaptic gain. We found, after comparing a large number of high quality recordings from different cells, that even at the same adapting background there is a large variation in the calculated synaptic gain (for example, a variation of 1.5 to 4.5 at a background of 500,000 photons/s). This was mainly due to variation in the size of the LMC responses and not of the presynaptic photoreceptor responses.

How do the dynamics of LMC responses change with increased light adaptation? We studied this question first by introducing a fixed set of contrast steps at different adapting backgrounds. Fig. 4 shows the records from one such experiment. At low backgrounds, the LMC responded to 300-ms contrast steps with relatively slow responses, but as the light intensity level was increased, the responses became more

transient as they rapidly decayed towards the plateau potential. This decay was faster and more prominent with hyperpolarizing on responses than with depolarizing off responses. The peak amplitudes of the on transients remained fairly constant, whereas the off transients (that were generally larger than the corresponding on

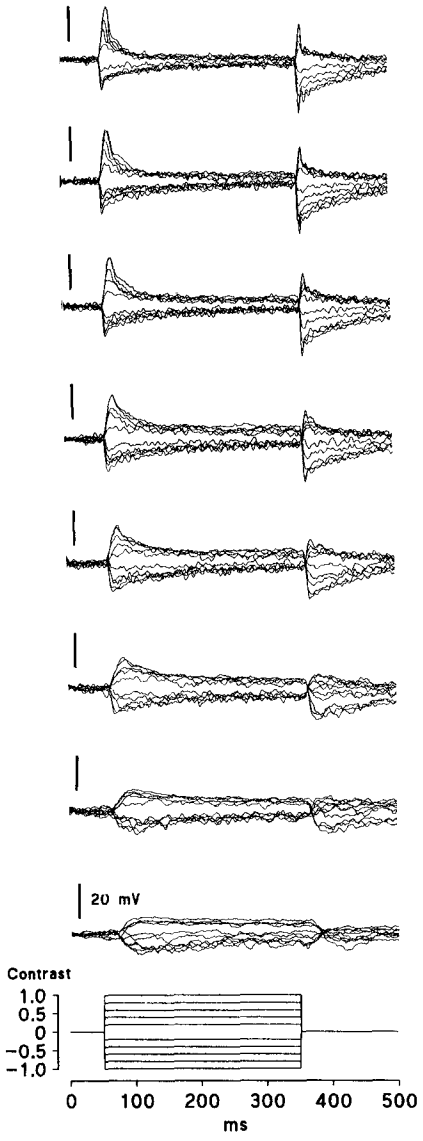

FIGURE 4. The effect of increased light adaptation on the wave form of LMC responses. Examples of LMC responses to a set of 300-ms contrast steps superimposed on eight different backgrounds 0.5 log intensity units apart, the highest background of ~500,000 photons/s. The responses became more transient as the background was increased.

transients) increased with the increase in the background intensity. If evaluated by the peak amplitudes, the contrast gain of the early visual signals increases with light adaptation. The estimates of synaptic gain will be refined in the following with the frequency domain analysis.

Responses to Pseudorandom Stimuli

Fig. 5 shows 30-times averaged samples of photoreceptor and LMC responses (i.e., signals) to a pseudorandomly modulated light stimulus (with the mean contrast of 0.32) at eight different adapting backgrounds. Unlike the responses to 300-ms contrast steps, the pseudorandomly modulated photoreceptor signals were much smaller than the LMC ones. This reduction in the size of the presynaptic signals can be explained by the fairly slow photoreceptor responses. Because the photoreceptors reach their maximum amplitudes ~ 15–30 ms after the light intensity is changed (cf.

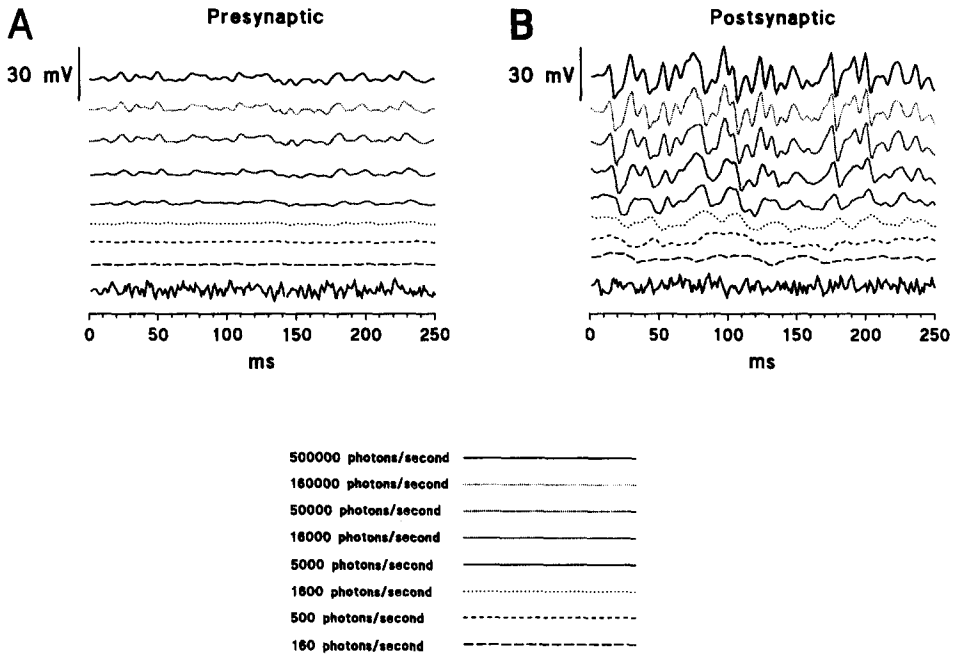

FIGURE 5. 250-ms samples of photoreceptor and LMC signals (30-times averaged responses) to a pseudorandomly modulated stimulus with a mean contrast of 0.32 (the lowest trace) at eight backgrounds, 0.5 log intensity units apart. The magnitude of both the photoreceptor and LMC signals is increased with adaptation. Numbers indicated in the line type decoder (under the figures) specify each mean light background, and the same line types are also used in the successive figures throughout the paper.

Fig. 3 *C;* light increments and decrements, respectively), the dynamically modulated intensity does not provide enough time for photoreceptors to generate as large responses as with long contrast steps (cf. Juusola, 1993). Thus, the presynaptic responses to pseudorandom stimuli exhibit mostly the raising phases of the long step responses. Interestingly, the LMC peak-responses were approximately as large as the ones elicited with contrast steps. In essence, this again demonstrates that small transient changes in the presynaptic signal are sufficient to provoke maximum postsynaptic responses.

The effect of increased light adaptation on the dynamics of the pre- and postsynaptic signals were next studied by calculating the amplitude distribution histograms of the signals and comparing these to the corresponding mean potentials of the cells.

The mean photoreceptor potential increased with background intensity and usually saturated 20–25 mV above the dark resting potential (Fig. 6 *B*) (Howard et

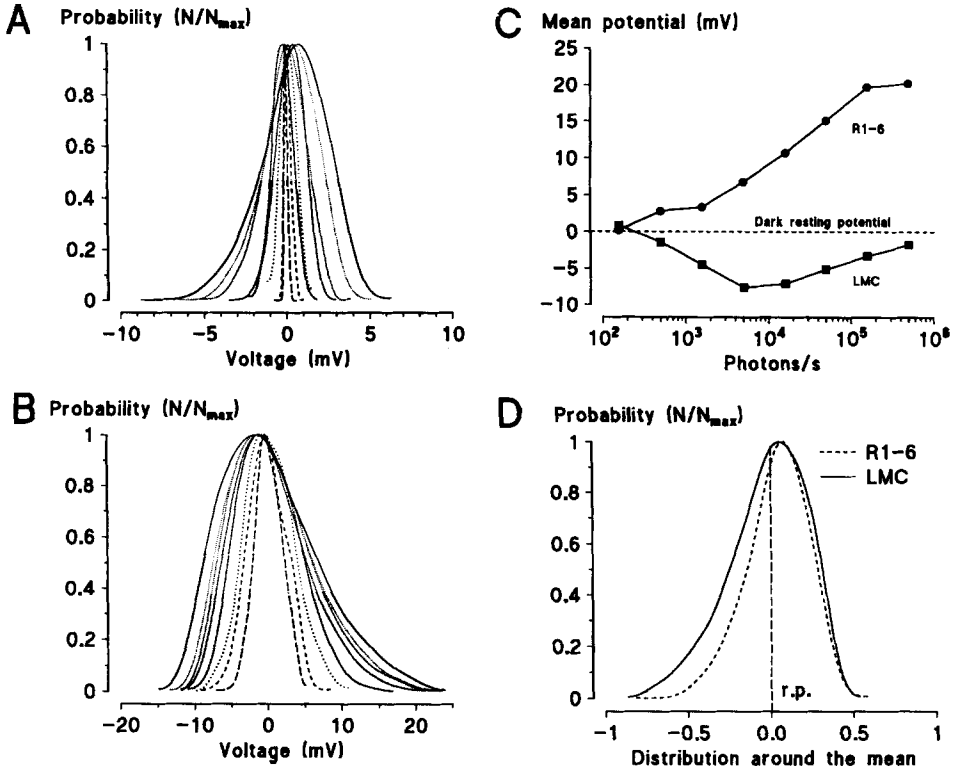

FIGURE 6. Changes in the distributions and means of the photoreceptor and LMC signals at different adapting backgrounds. Photoreceptor (*A*) and LMC (*C*) signal distributions scaled around the mean potential, 0, at different adapting backgrounds. (*B*) The corresponding mean photoreceptor and LMC potentials at different adapting backgrounds. (*D*) Comparison of the photoreceptor and LMC signal distributions at a background of 500,000 photons/s. The LMC signal distribution was inverted and both the distributions were scaled in order to match their means to demonstrate the overlap. Note how the positive contrasts overlap (amplified with constant gain), but the negative contrasts are more larger in the postsynaptic signals. All the histograms were smoothed with a five-point moving average.

al., 1987; Juusola, 1993). On the other hand, increasing the mean illumination hyperpolarized the LMCs (with large responses) at low backgrounds but depolarized the mean potential towards or beyond the dark resting potential at high backgrounds. Both the pre- and postsynaptic probability density functions (PDF) behaved similarly, changing from Gaussian distributions at low adapting backgrounds to

skewed ones at higher backgrounds (Fig. 6 *A*). Thus, the LMC signals, although inverted, mainly followed the photoreceptors with an amplification ratio (Fig. 6 *C*). However, as seen previously with step responses (Fig. 4), the amplification of depolarizing responses in LMCs (i.e. responses to light decrements) were often more enhanced. This is seen in Fig. 6 *D*, which illustrates both the pre- and the postsynaptic signal distributions at a background of ~500,000 photons/s, now scaled to the same width around their means. The increased postsynaptic enhancement of light decrements suggest voltage-dependent mechanisms in LMCs, i.e., larger off-transients after strong hyperpolarization (off spikes; Hardie and Weckström, 1990), or additional synaptic inputs.

Transfer Functions of the Photoreceptor and LMC

Fig. 7 illustrates the pre- and postsynaptic transfer functions, the coherence estimates and the linear impulse responses (first order Wiener kernels) calculated from the pseudorandomly modulated stimuli (mean contrast of 0.32) and the corresponding averaged voltage responses (i.e., signals) at different adapting backgrounds (Fig. 5). Neither pre- nor postsynaptic responses saturated during stimulation. This was tested by using smaller contrast amplitudes, which gave transfer functions of similar form (data not shown).

As the background intensity was increased, the photoreceptor gain (Fig. 7 *A*) increased its band width, shifting the 3-dB cut–off frequency towards higher values (as reported earlier by Juusola et al., 1994). In the corresponding LMC gain (Fig. 7 *B*), there was an increased attenuation of low frequencies accompanied by a very strong increase in the 3-dB cut-off frequency, reaching a value of 80 Hz at a background of ~500,000 photons/s. Although the general behavior of LMC transfer functions was consistent, the postsynaptic 3-dB cut–off frequency varied from cell to cell at the highest background (109.3 ± 28.9 Hz, mean ± SD, $n = 12$). This variation was somewhat related to the presence of the off spike or the oscillations in the step responses, as in cells with these features, high frequencies were boosted even more. At the two lowest backgrounds the shape of the photoreceptor and LMC gains were alike, but the overall LMC gain was much higher. Indeed, the changes in the 3-dB cut-off frequencies, (Fig. 8 *A*) illustrate similar pre- and postsynaptic values at these adapting backgrounds.

Both the photoreceptor and LMC phase lags were reduced by light adaptation (Figs. 7, *B* and *F*). At the lowest tested background the slow LMC responses followed the presynaptic signal by ~180°. Thus, during transmission, the signal was simply inverted with no further delay. However, the postsynaptic phase was reduced at higher backgrounds.

The coherence function is unity in a linear and totally noise-free system, and all nonlinearities and noise lower the value. According to the results in Fig. 7, *C* and *G* (and also photoreceptor coherence functions in Juusola et al., 1994) the pre- and postsynaptic signals were approximately linear ($\gamma^2 \geq 0.9$) over the frequency range from 0.5 to 150 Hz and from 5 to 150 Hz, respectively, at backgrounds >5,000 photons/s. The drop in LMC coherence at low frequencies apparently followed the light-adaptational reduction of the corresponding gain values. However, when we regard that the coherence function as an estimate of the system's linearity and

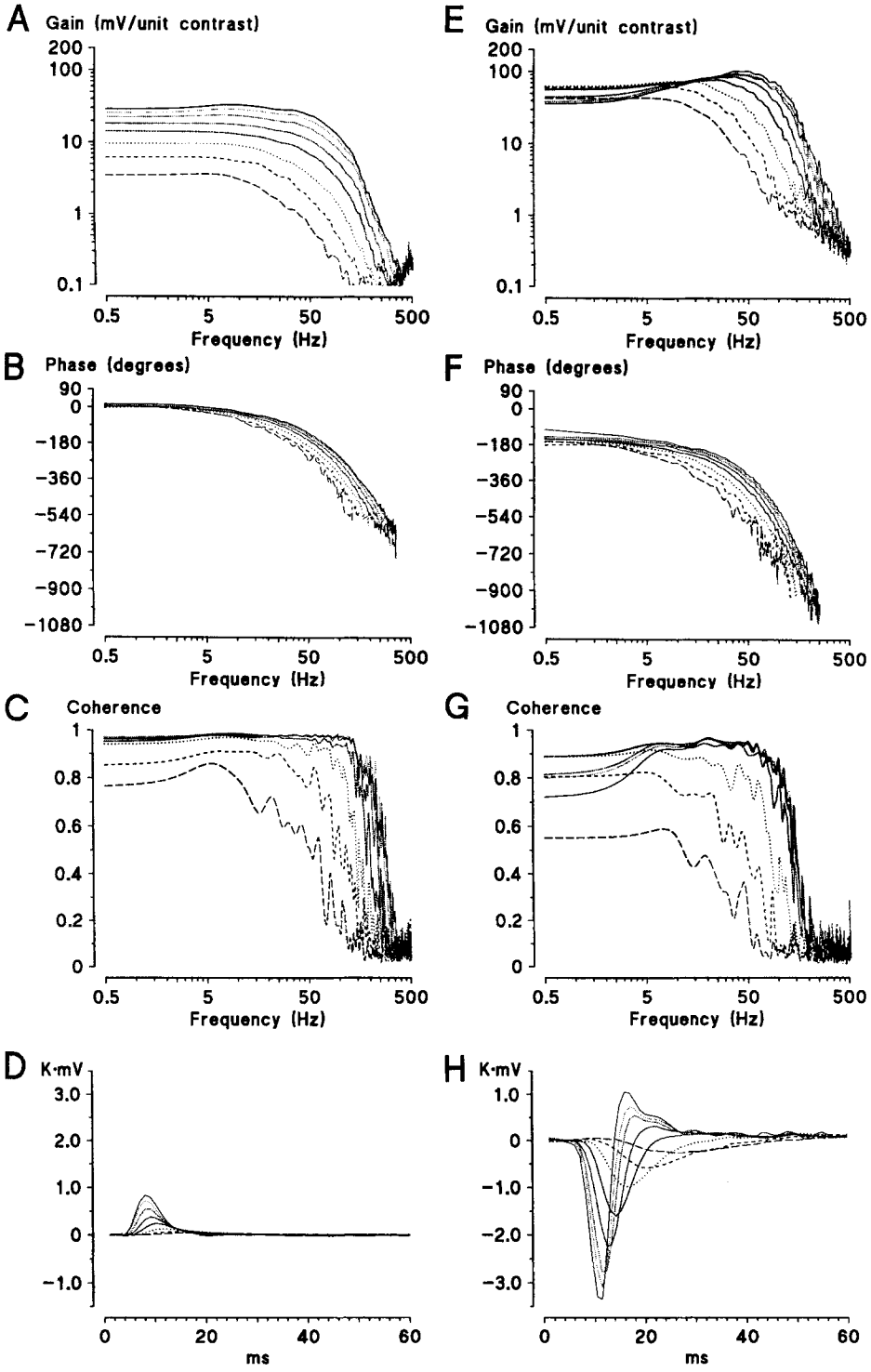

FIGURE 7. The photoreceptor and LMC frequency responses (gain and phase), their coherence functions and linear impulse responses at eight different adapting backgrounds. Photoreceptor data at left, LMC data at right.

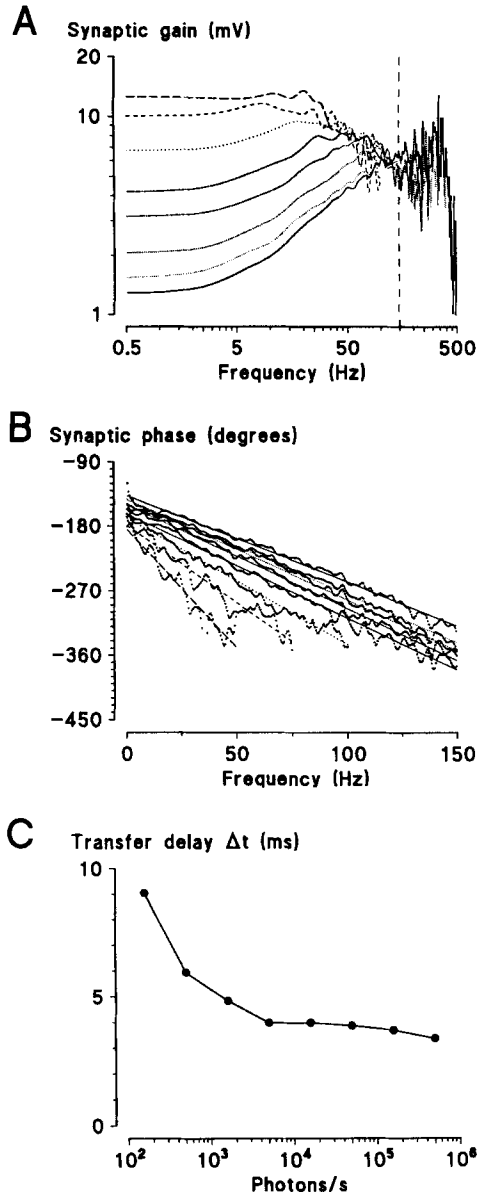

FIGURE 8. Parameters of signal transfer function calculated from the frequency responses. (*A*) The photoreceptor and LMC 3-dB cut–off frequencies at different adapting backgrounds. (*B*) Synaptic amplification calculated from the peak values of photoreceptor and LMC first-order Wiener kernels. (*C*) The time-to-peak of the photoreceptor and LMC first order Wiener kernels.

signal-to-noise ratio, and judge the amount of noise occurring both pre- and especially postsynaptically (as will be shown below), the linearity of the light-adapted cells was remarkable even under strong dynamic stimulation. Thus, we can say that within the frequency and light background limits stated above, the system under study, the synapse, behaves quite linearly. This also fully justifies the use of linear systems analysis within the same limits. We cannot say that all significant deviations from near unity coherence values are caused by the system's nonlinearities. On the

contrary, the most likely explanation for low coherence at low backgrounds and small frequencies is the poor SNR (see below).

The linear impulse responses (first order Wiener kernels; Fig. 7, *D* and *H*) demonstrated how both the pre- and postsynaptic responses increased as a function of light adaptation and that the presynaptic responses reached their peak values only few milliseconds earlier than the corresponding postsynaptic responses. Thus, the results coincide with the ones observed with 2-ms contrast steps (Fig. 3 *C;* for this particular LMC see Fig. 14 *C*). Here, the difference in the pre- and postsynaptic time-to-peak values was the smallest (2–3.5 ms) at the three highest adapting backgrounds and largest (11 ms) at the lowest background. Because the signals reached their maxima in a causal order, we could again estimate the synaptic amplification at different adapting backgrounds by simply dividing the postsynaptic maximum amplitudes by the corresponding presynaptic ones. These values are shown in Fig. 8 *C*. The increase of the background by 3.5 log intensity units caused ~2.5-fold reduction in the synaptic amplification (from ~10 to ~4). To observe what kind of frequency-dependent changes are caused by light adaptation in the different signal components and to estimate the average transfer delay at different backgrounds, we calculated the synaptic transfer functions.

Synaptic Transfer Function

The synaptic transfer functions in Fig. 9 *A* show the changes in the signal transfer over a wide frequency band at different adaptation conditions. At the lowest tested adapting background (~160 photons/s) there was ~13-fold amplification of low frequency signals after which the gain rolled off down to fourfold value at 60 Hz. Because of the low coherence value of LMCs at low intensity backgrounds, the higher frequencies were disregarded. Interestingly, as the background intensity increased, synaptic amplification was continuously reduced over the band of frequencies from 1 to 150 Hz (with coherence values between 0.60 and 0.98), although the greater effect was at low frequencies (cf. synaptic gain with one background in French and Järvilehto, 1978). For instance, at the highest background (~500,000 photons/s), the 1-Hz signal had an approximately unity gain. Above this the synaptic amplification increased steadily until ~150 Hz, after which the reliability of the estimate was too low to be significant (see LMC coherence values in Fig. 7 *G*). The change in gain in the synapse is in contrast with findings of Laughlin et al. (1987), who found, using step input, no change with light adaptation.

The phase parts of the synaptic transfer function, which are the difference between corresponding pre- and postsynaptic phases, attenuated slowly from low to high frequencies, so that the slope was smaller at stronger backgrounds (Fig. 9 *B*). The transfer delay of signals (i.e., the group delay, $-d\Phi/df$) at different adapting backgrounds was calculated from the regression lines used for fitting the phase function (correlation coefficient varied from 0.993 to 0.998). Fig. 9 *C* shows how the transfer delay reduced exponentially from 9 ms to 3.3 ms when the light background was increased from ~160 to ~500,000 photons/s (Fig. 9 *C*). The "inverse" time lag in time domain recordings with dark-adapted eye is clearly a manifestation of nonlinearities, which are bypassed with the white-noise stimulation, thus revealing the true synaptic lag.

Noise Analysis

Time domain. Fig. 10, *A* and *B*, shows samples of dark noise and the signal-induced noise in a photoreceptor and a LMC, respectively, at different adapting backgrounds. It is easily seen that the LMC noise is larger in amplitude than the photoreceptor noise. Yet both appear to behave similarly. The variance of the noise first increases

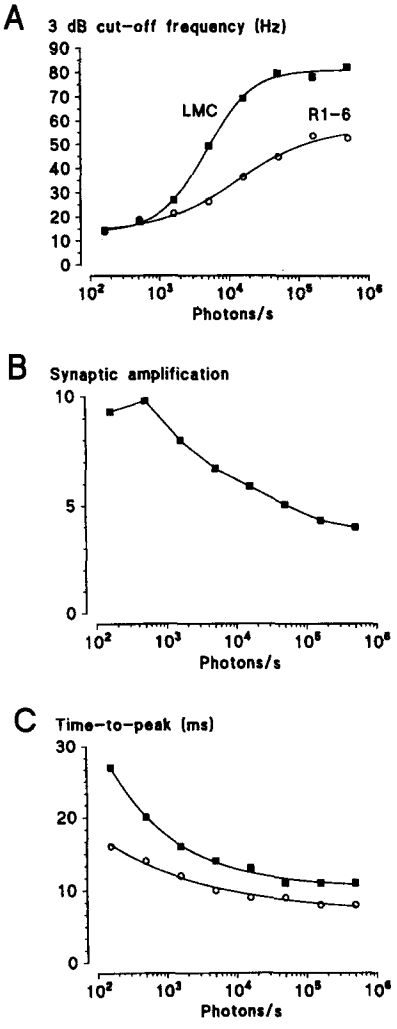

FIGURE 9. The synaptic transfer function and transfer delay at eight different adapting backgrounds. (*A*) The synaptic gain. (*B*) The synaptic phase plotted versus a linear frequency scale. (*C*) The transfer delay calculated from the synaptic phase function above.

then decreases with background intensity (Fig. 10 *C*), and finally returns near to the values of dark adapted cells (the lowest traces in Fig. 10, *A* and *B*). This inflection point in noise amplitude varied from cell to cell in both photoreceptors and LMCs.

Frequency domain. To see how the frequency content of the noise changed during adaptation, the power spectra of signal-induced photoreceptor and LMC noise were compared in dark and at different adapting backgrounds (Fig. 11). The

noise in both cell types showed a light adaptational shift of power over a wide frequency range. Photoreceptor noise power rose to a maximum at an adapting background of $1.7 \cdot 10^4$ photons/s, but decreased and shifted towards higher frequencies with more intense backgrounds (Fig. 11 *A*). This corresponds to the reduction of duration of single photon events reported previously (e.g., Wong, 1978; Howard et al., 1987; Roebroek, van Tjonger and Stavenga, 1990; Juusola et al., 1994). The

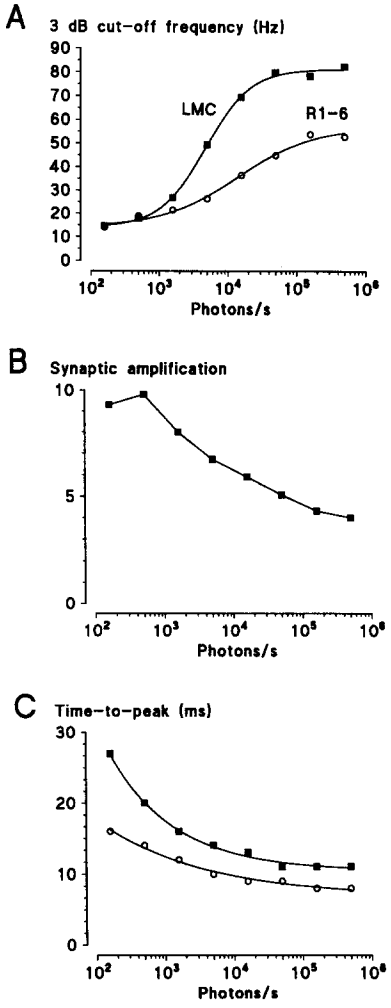

FIGURE 10. Noise analysis in the time domain. (*A* and *B*) 500-ms samples of signal-induced photoreceptor and LMC noise, respectively, in darkness (*lowest traces*) and at eight different adapting backgrounds 0.5 log intensity units apart. (*C*) The variance of photoreceptor and LMC noise calculated from the data shown in *A* and *B*. Each value is an average of 240, 1-s samples (for each of which the mean potential was first zeroed). For details of the analysis see Materials and Methods.

power at low frequencies (0.5–5 Hz) depended partially on the amount of slow, gradual fluctuations of the mean potential during experiment, and might have a contribution of the screening pigment movement. The amplitude of the fluctuation varied in different experiments and was usually $< \pm 1.0$ mV.

The LMC noise consists of the amplified photoreceptor noise and intrinsic noise associated with signal transfer (Laughlin et al., 1987). Because LMCs receive

information from six converging photoreceptor axon terminals, one might assume that the synaptic gain is merely due to this connectivity, and that its value must be fixed. However, if the photoreceptor-LMC synapse had a constant amplification ratio at all backgrounds, then the LMC noise power spectra would be parallel to the photoreceptor noise power with a maximum at the background of $1.7 \cdot 10^4$ photons/s. As already demonstrated by the synaptic transfer functions, this was not the case. The LMC noise power was largest at the lowest adapting background of 160 photons/s, above which it steadily decreased towards higher frequencies as the background was

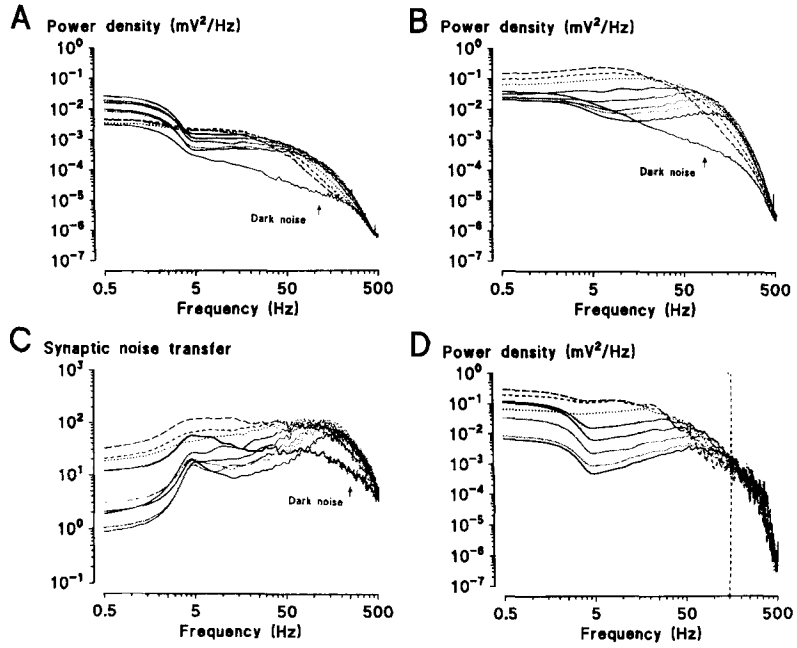

FIGURE 11. Noise analysis in the frequency domain. (*A*) Photoreceptor noise power spectra. (*B*) LMC noise power spectra. (*C*) Synaptic noise transfer in the dark and at eight different adapting backgrounds 0.5 log intensity units apart. (*D*) Transmitted photoreceptor noise. The dark noise is marked, the continuous line is at the adapting background of 500,000 photons/s. To recapitulate the calculation methods, the synaptic noise transfer is calculated by dividing LMC noise by photoreceptor noise power spectra (i.e., $C = B/A$), and the transmitted noise is derived by filtering photoreceptor noise by the synaptic transfer function (i.e., D is A filtered by the function of Fig. 9 *A*).

increased (Fig. 11 *B*). The synaptic noise transfer in Fig. 11 *C* shows that in darkness, and at the lowest tested adapting background, the synaptic noise transfer was fairly flat but showed increased compression of lower frequencies as the mean background was increased. The low frequency peak at 5 Hz was again related to the small fluctuations in the mean potentials in photoreceptors during the experiments.

The power spectrum of the intrinsic noise was estimated in the following way: the presynaptic noise was multiplied by the corresponding synaptic transfer function, using the pre- and postsynaptic gains from the same measurements, and the result

was divided by $\sqrt{6}$ (scales the noise of six converging photoreceptors). The presynaptic noise, after passing through the analogously light-adapted synapse, is shown in Fig. 11 *D*. The result resembles the LMC noise power spectra. We subtracted this estimated power of the synaptically modulated presynaptic noise from the corresponding real (recorded) LMC power spectra. This procedure gave an approximation of the intrinsic noise (Fig. 12 *A*), at least at the highest adapting backgrounds, where the estimate is most reliable. The intrinsic noise power was much greater than from a single photoreceptor at the same background (Fig. 10 *C*). It made up ~30% of the total power in the LMC noise spectrum. The 95% confidence intervals (see Appendix, Eq. 9) for the photoreceptor and LMC gain estimates are ~±0.5% and ±1.5%, respectively. This means that we have ~±2% confidence band for the synaptic transfer functions. The subtraction of the recorded LMC noise from the estimated transmitted noise results in a ~30% band for 95% confidence limits. Thus, it is still relatively reliable, although the variance of its estimate is considerable.

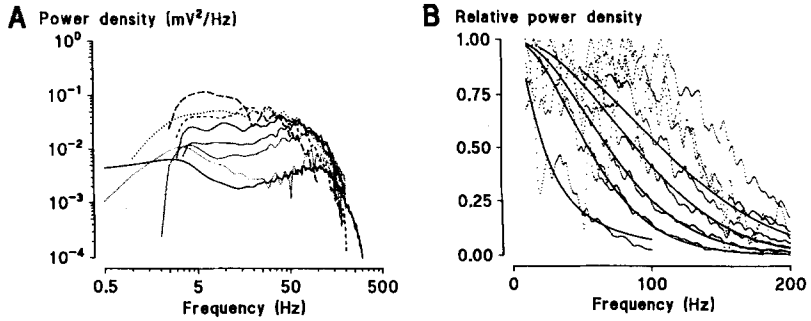

FIGURE 12. Intrinsic noise in an LMC at different adapting backgrounds. (*A*) The noise as derived by subtracting the transmitted noise from the real (measured) LMC noise (i.e., Fig. 11, *B–D*). (*B*) The same data shown in relative linear scale. The continuous lines represent best fits of the Eq. 11 (the gamma distribution) to the five lowest adapting backgrounds.

Fig. 12 *B* shows the synaptic intrinsic noise (relative) in linear scale. The continuous lines represent the least-squares fits of the Γ-distribution to the noise spectra with the lowest five adapting backgrounds. This procedure allows us to roughly estimate the duration of the elementary synaptic events, assuming that the events are caused by a diffusion limited process (e.g., release of transmitter vesicles and the subsequent diffusion in the synaptic cleft). The Γ-distribution gave a good fit (correlation coefficient >0.95) with the four lowest adapting backgrounds. With higher backgrounds the fit was poor, and no quantitative estimates can be made. However, going from the adapting background of 160 eph/s to 16,000 eph/s the time constant decreased from ~8 ms to ~0.1 ms. This suggests rapid shortening of the duration of the elementary synaptic responses as a function of the light intensity.

Pre- and Postsynaptic Signal-to-Noise Ratios

The photoreceptor and LMC SNR were calculated in the time domain from the signal and the signal-induced noise variances, and in the frequency domain from the power spectra of the same original data. The light adaptational increase in the SNRs

of both cells are shown in Fig. 13 *A*. Both the pre- and postsynaptic SNR as functions of background intensity seemed, as also found by Laughlin et al. (1987), to approximately follow the relation:

$$\mathrm{SNR} - k\sqrt{I} \tag{2}$$

where k is a proportionality constant, and I is the intensity of the adapting light. The changes in the frequency domain are illustrated in Fig. 13 *B* and *C*. At low adapting

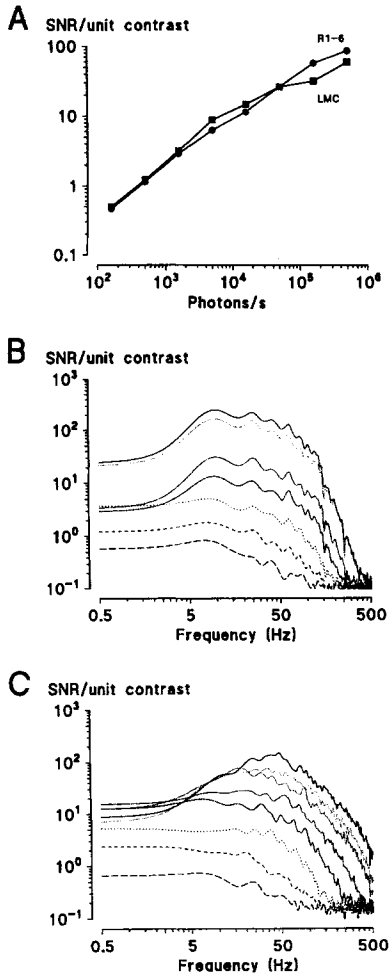

FIGURE 13. Photoreceptor and LMC signal-to-noise ratio at eight different adapting backgrounds. (*A*) SNR was calculated from the signal and noise variances of the corresponding pre- and postsynaptic data. (*B*) Photoreceptor SNR and C LMC SNR in the frequency domain.

background, the band widths were similar, but as the SNR increased rapidly with the background, both cell types demonstrated a characteristic reduction of the SNR at low frequencies. In general, LMCs had a higher SNR than the photoreceptors. At high frequencies (200–500 Hz), the coherence of the signals was near zero although the SNR was high, indicating that the system must be nonlinear at those frequencies.

This phenomenon could be related to oscillations characteristic of LMC responses (e.g., Fig. 2 *E* responses to 2 ms contrast steps and the upper trace in Fig. 4).

Recordings from Photoreceptor Axon Terminals

Responses from photoreceptor axons were identified by fast depolarizing transient superimposed on the rising phases of the photoresponses (Fig. 14 *A*) (Weckström et al., 1992*a*). When recording from fly lamina, stable microelectrode penetrations of axon terminals are difficult to perform. Because of the axons' small diameter (ø 1–2 μm), very sharp electrodes (over 250 MΩ) are required. However, we succeeded in recording the axon transfer function to pseudorandom contrast modulation three times. Fig. 14 *B* compares transfer functions from an axon terminal to the ones of the photoreceptor soma and LMC, recorded at an adapting background of 1,000,000 photons/s (with mean contrast of 0.32). It demonstrates how the axonal transfer

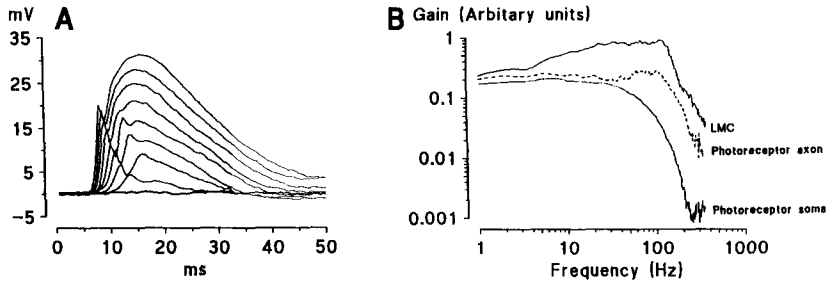

FIGURE 14. Photoreceptor axon recordings. (*A*) Responses to 2-ms light steps. (*B*) Frequency response of a photoreceptor axon terminal (*dashed line*) is compared to the ones of photoreceptor soma and LMC. Note how the axonal cut-off frequency corresponds to the one of the LMC.

function differs from the photoreceptor and has a corner frequency as high as an LMC. Indeed, the peak-to-peak responses during contrast modulation were only ±8 mV. Thus, the responses in the axon were much smaller than those of LMCs, but a little larger than in a typical photoreceptor soma.

DISCUSSION

The synaptic transmission of graded potentials from receptor cells to interneurons is a fundamental coding process that modifies the information content of the input. We chose to use the linear systems analysis to analyze this process. This is fully justified within a definite band of frequencies and in a restricted range of light backgrounds, because we could show the highly linear behavior of the synapse with the help of the coherence functions (Fig. 7, *C* and *G;* see also Eq. 5). In the present work we demonstrated that the photoreceptor-LMC synapse is an adaptive filter of which transfer function changes with background intensity. At low adapting backgrounds, the low-pass properties seem to be advantageous, but as the background is increased, the synaptic transfer function progressively acquires more and more band-pass properties.

In the following, we will discuss pre- and postsynaptic signal enhancement and the role that they play in maximizing the flow of information via the noisy channels of early vision. We will introduce a new descriptive model, based on the finding that the dynamics of tonic transmitter release change with the increased light adaptation (Fig. 12) and that contrast signals are mainly enhanced in the photoreceptor axon terminals (Fig. 14 *B*). The model is consistent with the present findings and the previous predictions (van Hateren, 1992*a,b*, 1993) about the dynamics of synaptic signal transfer at increased light adaptation: (*a*) change of synaptic transfer function from low-pass to band-pass; (*b*) decrease of synaptic gain; and (*c*) acceleration of postsynaptic LMC responses. We realize that there may be other synaptic inputs to LMCs besides the R1–6 photoreceptors. There is complex neural circuitry in the lamina, and many unknown processes may contribute to postsynaptic signal modulation (Strausfeld, 1976). Although the exact function of laminar neural circuitry is unknown, black box analysis, where photoreceptor input is the source of information, provides one approach to this problem.

Amplification of the Signal Changes in Light Adaptation

The gain of the photoreceptor-LMC synapse depends on the background (Fig. 9 *A*). Light adaptation increases the overall contrast gain of both the pre- and postsynaptic signals (Figs. 4 and 6, *A* and *C*), but decreases both the synaptic gain and the transfer delay (Fig. 9, *A* and *C*). Adaptational changes in the synaptic gain primarily affect transmission of low frequencies. What are the mechanisms responsible for this regulation of signal amplification?

According to Nicol and Meinerzhagen (1982) ~1,200 structural synapses transmit the signals from six photoreceptors to one LMC. The summed activity of these synaptic terminals creates the postsynaptic responses. Light increments increase, and light decrements decrease, the release of the transmitter from the photoreceptor axon terminals (Laughlin and Osorio, 1989; Weckström, Kouvalainen, Djupsund, and Järvilehto, 1989). Binding of the transmitter, histamine, to the postsynaptic chloride channels modulates the chloride conductance (Hardie, 1987; Zettler and Straka, 1987; Hardie, 1989), and is mostly responsible for the on and off responses in LMCs (Laughlin and Osorio, 1989). To respond without saturation, the synapse must have mechanisms which rapidly return the potentials back to the mean or resting level (see Figs. 4 and 5 *B*). Our knowledge of the properties of the histamine-gated chloride channels (Hardie, 1989), and the present results, lead to the basic assumption that most information processing takes place before the chloride channels are activated, i.e., on the presynaptic side.

Presynaptic Mechanisms

The power spectra and variance of the LMC noise indicates that, even in darkness, there is tonic transmitter release affecting LMCs (Laughlin et al., 1987; Uusitalo and Weckström, 1994). Increased light adaptation drives the synaptic transfer function and intrinsic noise towards higher frequencies and compresses low frequencies (Figs. 9 and 11 *B*), suggesting that the elementary process of synaptic transmission speeds up. The mean photoreceptor potential follows the background illumination and probably mediates the change in tonic transmitter release. The finding that the

intrinsic noise also shifts to higher frequencies with light background (Fig. 12) suggests that the size of the functional transmitter packages—not necessarily equivalent with physical vesicles—gets smaller. This would explain the previous finding that the total amount of transmitter released does not seem to increase as a function of light adaptation, as tested by measuring the input resistance of LMCs (Laughlin and Osorio, 1989). Thus, our results indicate that the amount of transmitter released tonically seems fairly constant, but its effective quantal size is reduced.

In our previous work we have demonstrated a fast depolarizing transient in the photoreceptor axon terminals (Fig. 14 *A*), the kinetics of which well predicts the time course of postsynaptic on transients in the dark-adapted state (Weckström et al., 1992*a*). Because of photoreceptor geometry, with a large, leaking soma connected to a narrow axon that has a large input resistance, the fast depolarizing transient cannot be seen in the soma recordings (cf. van Hateren, 1986; Weckström et al., 1992*a*). Based on recent studies of other insect photoreceptors (Rubinstein, Bar-Nachum, Selinger, and Minke, 1989; Stockbridge and Ross, 1984; Coles and Schneider-Picard, 1989; Weckström, Järvilehto, and Heimonen, 1993) we presume that the spikelike fast depolarizing transients originate from the activation of voltage-dependent calcium or sodium channels. It is also functional when the photoreceptors are light adapted (Fig. 14 *B;* see also contrast steps in Weckström et al., 1992*a*). Our findings indicate that, since the enhancement of LMC responses coincided with the rising or decreasing phase of the photoreceptor responses (Fig. 3 *C*), the activation and deactivation of channels responsible for the fast depolarizing transient must be tuned to respond to even small changes from the mean photoreceptor potential. The purpose of the fast depolarizing transient mechanism is probably to amplify and separate the contrast signals from the mean potential by generating large voltage-changes that can transiently increase the amount of transmitter released. In other words it could be a separate "contrast enhancer"-unit that changes transmitter release by driving potential commands into the voltage-dependent "transmitter-releasing" unit. Because both fast depolarizing transient and tonic transmitter release are voltage-sensitive processes, their combined operation define the dynamics of transmitter release. It appears that changes in transmitter release take place more slowly at low backgrounds, where the mean photoreceptor potential is low and the photoresponses slow.

The descriptive model of adaptive regulation in signal transfer is illustrated in Fig. 15. Presynaptic amplification is defined here as the sum of enhanced contrast response (fast depolarizing transient superimposed on a photoreceptor response) and the tonic rate of transmitter release. At low adapting backgrounds, where the slow tonic transmitter release dominates LMC responses, the fast depolarizing transient, elicited by the rising (depolarizing) photoreceptor responses, must have a large gain to separate the contrast information from the large synaptic noise (cf. Figs. 8 *B* and 9 *A* [*upper trace*]). As the resulting signal, which now has an enhanced presynaptic gain, goes through the synapse, the transmitter release mechanism low-pass-filters the transmitter signal (Fig. 9 *A*), and removes most of the high frequency noise (cf. Fig. 12). Contrast responses superimposed on a low mean photoreceptor potential are so small (cf. Juusola, 1993) that, without the transient

enhancement, they would only marginally alter the near tonic release of transmitter and would therefore be contaminated by the intrinsic noise. Hence, the resulting amplified LMC responses resemble those of low-pass filtered photoreceptors (cf. *lower traces* of Figs. 7, *A* and *E*).

At high adapting backgrounds the synaptic amplification strategy is different. In photoreceptors, the increased contrast gain enhances the signal and increases the

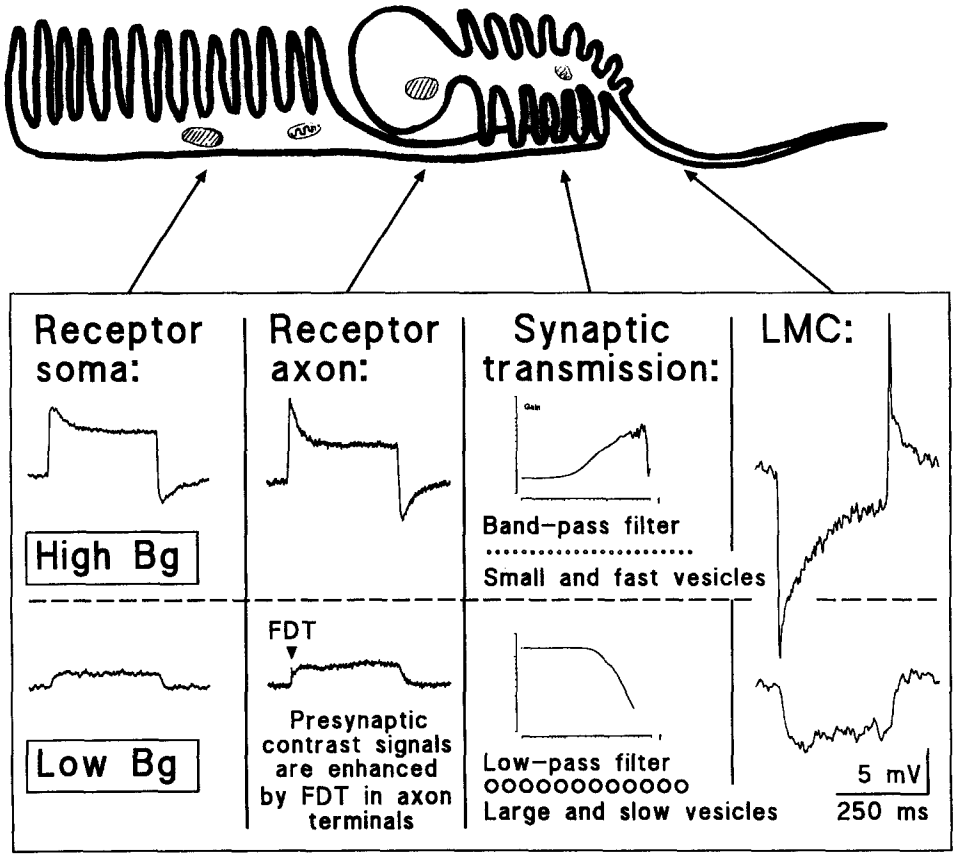

FIGURE 15. Schematic representation of the presynaptic modulation of the signal transfer at two light backgrounds (*Bg*), low (twilight) and high (near daylight). (*Round symbols*) Appearing below the synaptic transmission figures describe the changes in the effective size of the functional synaptic packets, not necessarily corresponding to actual vesicles.

SNR (Howard et al., 1987; Juusola, 1993; Juusola et al., 1994) so that the synaptic low-pass filtering is no longer needed. The photoreceptor potential is increased so that even small photoresponses, with fast depolarizing transients, can modulate the tonic transmitter release without the signal being heavily filtered (Figs. 9 *A* and 14 *B*). This is because the modulation of transmitter release at high presynaptic potentials is fast (cf. Fig. 12, *the continuous line*). The resulting LMC responses have a large high frequency content, characteristic for band-passed signals (Figs. 7 *E*, 8 *A*, and 14 *B*).

Further, it is essential to provide a large operation range for the postsynaptic responses without saturating the signal. Hence, as the presynaptic contrast gain increases (Fig. 7 *A*), the synaptic gain decreases as a function of light adaptation (Figs. 8 *B* and 9 *A*). This could be due to the properties of the presynaptic Ca^{2+} channels. In synapses between spiking cells in vertebrates they have been suggested to be mostly N-type channels that inactivate rapidly with depolarizing membrane potential (cf. Miller, 1987). However, recent evidence suggests, that in graded potential synapses the Ca^{2+} channels do not inactivate substantially, either in vertebrate photoreceptors (see e.g., Corey, Dubinsky, and Schwartz, 1984), bipolar cells (Kaneko, Pointo, and Tachibana, 1989) or in barnacle photoreceptors (Hayashi and Stuart, 1993). Thus, it does not seem likely that the synaptic gain in fly compound eye would be caused by the properties of the Ca^{2+} channels.

The reduction of synaptic gain seems to be a direct result of the reduction of low frequencies when the adapting background is increased. This subtraction is an efficient way to enhance the relative signal power at significant frequencies. At present the only mechanism capable of doing this is the generation of low-passed field potentials in the extracellular space inside the synaptic cartridge (Shaw, 1984). This subtraction mechanism (Laughlin and Hardie, 1978) would obviously also reduce the low frequencies which have the same frequency content as the field potential.

Another contribution may come from voltage-dependent potassium channels which effectively compress large depolarization responses, broadening the operational range for the presynaptic contrast responses (Laughlin and Weckström, 1989; Weckström, Hardie, and Laughlin, 1991; Weckström, Kouvalainen, and Juusola, 1992*b;* Juusola, 1993; Juusola and Weckström, 1993). K^+ channels may create a current sink near the axon origin, or they could be distributed along the axonal membrane as well. The presynaptic compression by voltage-dependent K^+-channels, when the presynaptic potential is depolarized, should influence the on responses preferentially. This is exactly what we have found. The adaptational change of the synaptic gain is associated with the increased skewness of the pre- and postsynaptic response histograms (Fig. 6, *A* and *C*).

Postsynaptic Mechanisms

The photoreceptor transmitter, histamine, activates Cl^--channels (Hardie, 1989), which may desensitize with a slow time constant (Roger Hardie, personal communication). Thus, they probably cannot be responsible for the fast transient generation, although the desensitization could be part of the slow gain regulation in the synapse. However, according to Hardie (1989), there are at least four histamine sites on one channel that must be filled before the channel can open. The high cooperativity makes the dose-response curve very steep. With tonic transmitter release the binding sites are always partially filled. Thus, a small modulation in transmitter release opens or closes a large number of chloride channels, i.e., amplifies the presynaptic signal. Additionally, the transmitter may be taken up quickly into the axons or glial elements. The explanation of the off-transient cannot solely be based on the closing of the transmitter-gated channels, because cutting off of the tonic transmitter release can only depolarize the cell by < 10 mV, and the off transient is also associated with

a conductance increase (Laughlin and Osorio, 1989; Weckström et al., 1992*a*). Therefore, off depolarizations must be enhanced by some other mechanism. One possible candidate is a nonhistamine-gated voltage–dependent depolarizing conductance (Hardie and Weckström, 1990; Laughlin and Osorio, 1989; Weckström et al., 1989; Uusitalo, Juusola, and Weckström, unpublished observations). The depolarization of the E_{Cl} of the postsynaptic LMC's due to intracellular Cl^--accumulation in light adaptive conditions (Uusitalo and Weckström, 1994) may also decrease the contrast responses with slow time course. This explains at least part of the drop in coherence of the LMC signals at low frequencies.

Concluding Remarks

The present study demonstrates two important properties of the fly photoreceptor-interneuron synapse, namely the strong adaptation of the transfer function, and the amazingly linear transformation taking place when white-noise modulated pointlike light stimulus is used. The skewness of the responses elicited by a Gaussian light stimulus (Fig. 6) implies that the signal amplification may have evolved to match the contrast distribution of natural scenes (which is also skewed, but in the opposite direction; Laughlin, 1981*b*). By compressing the responses evoked by positive contrasts (which extend to much higher values than the maximum negative contrasts of -1) and increasing the amplification of responses to negative contrast changes, the early visual system can map the natural contrast distribution with equal probability. Synaptic signal processing may thus efficiently maximize the amount of sensory information that can be transmitted to the central nervous system and select information that is significant for the animal's behavior (cf. animal's motion relative to the natural contrast distribution: van Hateren, 1992*a*,*b*, 1993).

APPENDIX

Analysis of the Pseudorandom Data

Fig. 16 illustrates the signal analysis using pseudorandomly modulated stimuli. The photoreceptor and LMC responses were recorded under identical stimulation conditions (The same contrast modulation was used at eight different adapting backgrounds). Data processing was done using ASYST 4.0 (Keithley Metrabyte, Taunton, MA) based programs (Juusola, 1993; Juusola et al., 1994; Kouvalainen et al., 1994). In the following, italicized text refers to the boxes in Fig. 16.

Time domain analysis. The purpose of this part of the analysis was to separate the signal from the noise. Responses to an identical stimulus sequence were averaged, and the averaged response were subtracted from the individual response samples to yield sequences containing only noise. 30 photoreceptor and LMC *Responses* to the same eight second stimulus sequence were recorded and stored. *Averaged responses* [$S_R(t)$ and $S_{LMC}(t)$] were calculated and subtracted separately from each of the stored nonaveraged response of the same cell [$R_R(t)$ and $R_{LMC}(t)$] to yield (30) 8-s samples of stimulus induced noise [$N_R(t)$ and $N_{LMC}(t)$; see the box between *Photoreceptor noise* and the *LMC noise*].

$$N_{LMC}(t) = R_{LMC}(t) - S_{LMC}(t). \quad (3)$$

The resulting noise samples, containing both the background and the modulation-induced noise, were stored for frequency domain analysis of the noise. The errors in this analysis, due to the residual noise in averaged responses, can be shown to be quite small, and proportional to noise power/$\sqrt{30}$ (Kouvalainen et al., 1994).

Frequency domain analysis of the signal. The linear dynamics of the signal transfer in the synapse were calculated from the transfer functions of the presynaptic photoreceptors and the postsynaptic LMCs, by treating the presynaptic signal as an

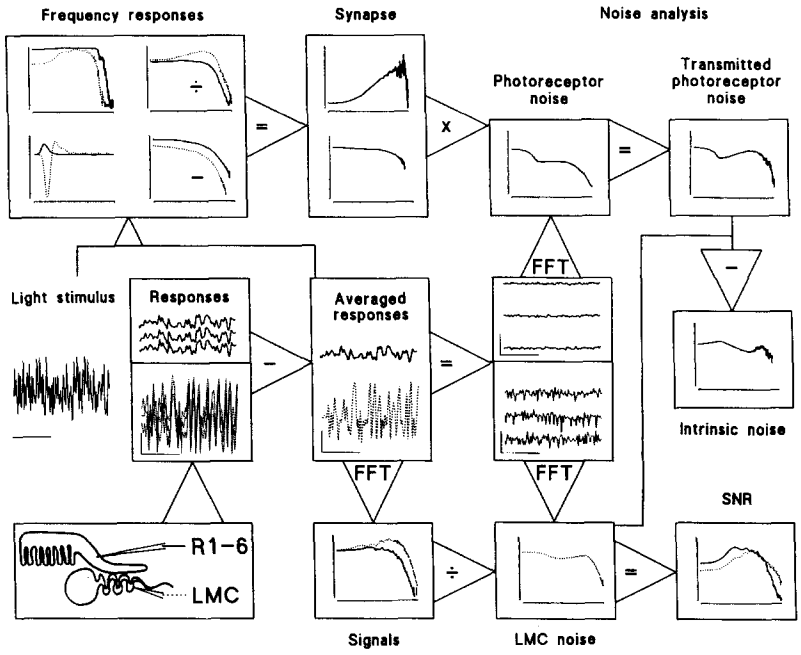

FIGURE 16. Schematic drawing of the analysis performed with pseudorandom contrast stimulation experiments. As indicated beside the schematic cells (*left, bottom*), continuous line is photoreceptor data, dotted line is LMC data throughout the figure. The Appendix gives a detailed description of the method. Shortly, the stimulus is provided by repeated sequences of pseudorandomly modulated light. The responses are averaged in time domain to give the *Signals*. Frequency domain data are obtained by standard FFT techniques. Transfer function analysis (*Frequency responses*) is performed using the signals of both photoreceptors and LMCs, and the synaptic transfer function (*Synapse*) is subsequently derived from these. Noise data is extracted by subtracting the averaged data from the original recordings, resulting in the estimation of the (*Intrinsic noise*) of the synapse.

input to the synapse. The averaged photoreceptor and LMC responses, containing virtually no stimulus-independent noise, were segmented for FFT analysis using a Blackman-Harris four-term window with 50% overlap of the segments (Harris, 1978; Bendat and Piersol, 1971). Photoreceptor and LMC *Signals* [$S_{R1-6}(f)$ and $S_{LMC}(f)$] were calculated by frequency domain averaging of the photoreceptor and LMC spectra of different segments. Thereafter, the photoreceptor and LMC *Frequency responses* [$H_{R1-6}(f)$ and $H_{LMC}(f)$] with coherence estimates and the first order Wiener

kernels (or linear impulse responses) were calculated by using the spectra of the *Light stimulus* and the *Averaged responses* (see, e.g., French, Holden, and Stein, 1972; Bendat and Piersol, 1971; Marmarelis and Marmarelis, 1978). The synaptic transfer function, *Synapse* [$H_S(f)$], was estimated by dividing $H_{LMC}(f)$ with $H_{R1-6}(f)$ recorded at the same background with the same contrast modulation.

$$H_S(f) - \frac{H_{LMC}(f)}{H_R(f)}. \tag{4}$$

The coherence functions were calculated as defined (Bendat and Piersol, 1971) as

$$\gamma^2(f) = \frac{\overline{G_{xy}}(f)\overline{G_{xy}}^*(f)}{\overline{G_{xx}}(f)\overline{G_{yy}}(f)} \tag{5}$$

where G_{xy} and G^*_{xy} are the cross-spectrum and its complex conjugate, correspondingly; G_{xx} is the input power spectrum and G_{yy} is the output power spectrum of the system being analyzed (the lower indices indicating the data from which the calculation is being made, x denotes input and y is output).

Frequency domain analysis of the noise. The intrinsic noise of the synapse, i.e., the noise produced during synaptic transmission itself, was estimated by taking the presynaptic noise through the synaptic transfer function, and comparing this to the real, recorded postsynaptic noise.

We calculated the photoreceptor noise power spectrum and the LMC power spectrum from the 30 stored samples of the signal-induced photoreceptor and LMC noise using standard FFT methods (see above) to obtain 30 estimates of the photoreceptor and LMC power spectra. The final estimates of the *Photoreceptor noise* power spectrum [$N_R(f)$] and the *LMC noise* power spectrum [$N_{LMC}(f)$] were averages (in the frequency domain) of the individual noise power estimates. To estimate the *Intrinsic noise* [$N_I(f)$;] we first estimated the *Transmitted photoreceptor noise* [$N_{LR}(f)$] by filtering the photoreceptor noise power spectra, $N_R(f\ )$, with the synaptic transfer function, $H_S(f)$, (estimated at the same background) and dividing that by the square root of six, because noise power in each LMC is reduced by uncorrelated noise input from six identical photoreceptors). Thus,

$$N_{LR}(f) = \frac{H_S(f) \cdot N_R(f)}{\sqrt{6}} \tag{6}$$

The *Intrinsic noise*, $N_I(f)$, was then calculated by subtracting the *Transmitted photoreceptor noise* power spectra, $N_{LR}(f)$ from the *LMC noise* power spectra, $N_{LMC}(f)$.

$$N_I(f) = N_{LMC}(f) - N_{LR}(f). \tag{7}$$

Calculation of the synaptic SNR. The photoreceptor and LMC signal-to-noise ratio, SNR, [$SNR_R(f)$ and $SNR_{LMC}(f)$], at a certain adapting background was determined by dividing the signal power spectrum of the cell, $S_R(f)$ or $S_{LMC}(f)$, by its noise power spectrum, $N_R(f)$ or $N_{LMC}(f)$ (See Kouvalainen et al., 1994; Juusola et

al., 1994).

$$SNR_{LMC}(f) = \frac{S_{LMC}(f)}{N_{LMC}(f)} \tag{8}$$

Calculation of the confidence intervals. The calculation of the noise components involves arithmetical operations with spectral and gain function estimates. These calculations necessarily decrease the reliability of the resulting functions, like the intrinsic noise. Therefore, it is necessary to estimate the confidence intervals of the relevant gain functions to find out, how useful the results are. We calculated the confidence intervals for the gain function according to Bendat and Piersol (1971) as

$$r^2(f) = \frac{2}{(n-2)} F_{2,n-2;\alpha}[1 - \gamma^2(f)] \frac{G_{yy}(f)}{G_{xx}(f)} \tag{9}$$

where n is the number of degrees of freedom, $F_{2,n-2;\alpha}$ is 100α percentage point of an F distribution with 2 and $n - 2$ degrees of freedom.

Calculation of the gamma distribution. The intrinsic noise in the synaptic transmission was assumed to arise (analogously with the single photon responses in photoreceptors; Wong, Knight, and Dodge, 1982, Juusola et al., 1994) from a diffusion-limited process following the Γ-distribution

$$\Gamma(t; n, \tau) = \frac{1}{n!\tau}\left(\frac{t}{\tau}\right)^n e^{-t/\tau}. \tag{10}$$

The two parameters, n and τ, were obtained by fitting the following to the experimental power spectra of the noise:

$$[\Gamma(f; n, \tau)]^2 = \frac{1}{(1 + (2\pi\tau f)^2)^{n+1}} \tag{11}$$

where f is the frequency.

We thank Eero Kouvalainen, Mika Laine, and Roger Hardie for critical reading of the manuscript.

Original version received 15 June 1994 and accepted version received 20 September 1994.

REFERENCES

Autrum, H.-J., F. Zettler, and M. Järvilehto. 1970. Postsynaptic potentials from a single monopolar neuron of the ganglion opticum I of the blowfly *Calliphora*. *Zeitschrift für Vergleichende Physiologie.* 70:414–424.

Bendat, J. S., and A. G. Piersol. 1971. Random Data: Analysis and Measurement Procedures. Wiley Interscience, New York. 407 pp.

Coles, J. A., and G. Schneider-Picard. 1989. Amplification of small signals by voltage-gated sodium channels in drone photoreceptors. *Journal of Comparative Physiology A.* 165:109–118.

Corey, D. B., J. M. Dubinsky, and E. A. Schwartz. 1984. The calcium current in inner segments of rods from the salamander (*Ambystoma tigerium*) retina. *Journal of Physiology.* 345:557–575.

Dubs, A., S. B. Laughlin, and M. V. Srinivasan. 1981. Single photon signals in fly photoreceptors and first order interneurones at behavioural threshold. *Journal of Physiology.* 317:317–334.

French, A. S. 1980*a*. Coherence improvement in white noise analysis by the use of a repeated random sequence generator. *IEEE Transactions of Biomedical Engineering.* 27:51–53.

French, A. S. 1980*b*. Phototransduction in the fly compound eye exhibits temporal resonances and a pure time delay. *Nature*. 283:200–202.

French, A. S., A. V. Holden, and R. B. Stein. 1972. The estimation of a frequency response function of a mechanoreceptor. *Kybernetik*. 11:15–23.

French, A. S., and M. Järvilehto. 1978. The transmission of information by first and second order neurons in the fly visual system. *Journal of Comparative Physiology A*. 126:87–96.

French, A. S., M. Korenberg, M. Järvilehto, E. Kouvalainen, M. Juusola, and M. Weckström. 1993. The dynamic nonlinear behavior of fly photoreceptors evoked by a wide range of light intensities. *Biophysical Journal*. 65:832–839.

Hardie, R. C. 1987. Is histamine a neurotransmitter in insect photoreceptors? *Journal of Comparative Physiology A*. 161:201–213.

Hardie, R. C. 1989. A histamine-gated chloride channel involved in neurotransmission at a photoreceptor synapse. *Nature*. 339:704–707.

Hardie, R. C., and M. Weckström. 1990. Three classes of potassium channels in large monopolar cells of the blowfly *Calliphora vicina*. *Journal of Comparative Physiology A*. 167:723–736.

Harris, F. J. 1978. On the use of the windows for harmonic analysis with the discrete Fourier transform. *Proceedings of the IEEE*. 66:51–84.

Hayashi, J. H., and A. E. Stuart. 1993. Currents in the presynaptic terminal arbors of barnacle photoreceptors. *Visual Neuroscience*. 10:261–270.

Howard, J., B. Blakeslee, and S. B. Laughlin. 1987. The intracellular pupil mechanism and the maintenance of photoreceptor signal to noise ratios in the blowfly *Lucilia cuprina*. *Proceedings of the Royal Society of London*. 231:415–435.

Juusola, M. 1993. Linear and nonlinear contrast coding in light adapted blowfly photoreceptors. *Journal of Comparative Physiology A*. 172:511–521.

Juusola, M., and M. Weckström. 1993. Band-pass filtering by voltage-dependent membrane in an insect photoreceptors. *Neuroscience Letters*. 154:84–88.

Juusola, M., E. Kouvalainen, M. Järvilehto, and M. Weckström. 1994. Contrast gain, signal-to-noise ratio and linearity in light-adapted blowfly photoreceptors. *Journal of General Physiology*. 104:593–621.

Järvilehto, M., and F. Zettler. 1971. Localized intracellular potentials from pre- and postsynaptic components in the external plexiform layer of an insect retina. *Zeitschrift der Vergleichende Physiologie*. 75:422–440.

Järvilehto, M., and F. Zettler. 1973. Electrophysiological-histological studies on some functional properties of visual cells and second order neurons of an insect retina. *Zeitschrift der Zellforschung*. 136:291–306.

Kaneko, A., L. H. Pointo, and M. Tachibana. 1989. Transient calcium current of retinal bipolar cells of the mouse. *Journal of Physiology*. 410:613–629.

Kirschfeld, K. 1967. Die Projektion der optischen Umwelt auf das Raster der Rhabdomere im Komplexauge von Musca. *Experimental Brain Research*. 3:248–270.

Koshland, D. E., A. Goldbeter, and J. B. Stock. 1982. Amplification and adaptation in regulatory and sensory systems. *Science*. 217:220–225.

Kouvalainen, E., M. Weckström, and M. Juusola. 1994. Determining photoreceptor signal-to-noise ratio in the time and frequency domains with a pseudorandom stimulus. *Visual Neuroscience*. 11:1221–1225.

Laughlin, S. B. 1981*a*. Neural principles in the peripheral visual system of invertebrates. *In* Handbook of Sensory Physiology. Vol. VII/6B. H. Autrum, editor. 133–280.

Laughlin, S. B. 1981*b*. A simple coding procedure enhances a neuron's information capacity. *Zeitschrift der Naturforschung C*. 36:910–912.

Laughlin, S. B. 1987. Form and function in retinal processing. *Trends in Neurosciences.* 10:478–483.

Laughlin, S. B. 1989. The role of sensory adaption in retina. *Journal of Experimental Biology.* 146:39–62.

Laughlin, S. B., and R. C. Hardie. 1978. Common strategies for light adaptation in the peripheral visual systems of fly and dragonfly. *Journal of Comparative Physiology A.* 128:319–340.

Laughlin, S. B., J. Howard, and B. Blakeslee. 1987. Synaptic limitations to contrast coding in the retina of the blowfly *Calliphora. Proceeding of Royal Society of London B.* 231:437–467.

Laughlin, S. B., and D. Osorio. 1989. Mechanisms for neural signal enhancement in the blowfly compound eye. *Journal of Experimental Biology.* 144:113–146.

Laughlin, S. B., and M. Weckström. 1989. The activation of slow voltage-dependent potassium conductance is crucial for light adaptation in blowfly photoreceptors. *Journal of Physiology.* 418:200*P.* (Abstr.)

Marmarelis, P. Z., and V. Z. Marmarelis. 1978. Analysis of physiological systems: the white noise approach. Plenum Publishing Corp., New York.

Miller, R. J. 1987. Multiple calcium channels and neuronal function. *Science.* 235:46–52.

Nicol, D., and I. A. Meinertzhagen. 1982. An analysis of the number and composition of the synaptic populations formed by photoreceptors of the fly. *Journal of Comparative Neurology.* 207:29–44.

Roebroek, J. G. H., M. van Tjonger, and D. G. Stavenga. 1990. Temperature dependence of receptor potential and noise in fly (*Calliphora erythrocephala*) photoreceptor cells. *Journal of Insect Physiology.* 36:499–505.

Rubinstein, C. T., S. Bar-Nachum, Z. Selinger, and B. Minke. 1989. Light-induced retinal degeneration in rdgB (retinal degeneration B) mutant of *Drosophila:* Electrophysiological and morphological manifestations of degeneration. *Visual Neuroscience.* 2:529–539.

Shapley, R., and C. Enroth-Cugell. 1984. Visual adaptation and retinal gain controls. *Progress in Retinal Research.* 3:263–346.

Shaw, S. R. 1984. Early visual processing in insects. *Journal of Experimental Biology.* 112:225–251.

Stockbridge, N., and W. N. Ross. 1984. Localized Ca^{2+} and calcium-activated potassium conductances in the terminals of a barnacle photoreceptor. *Nature.* 309:266–268.

Strausfeld, N. J. 1971. The organization of the insect visual system (light microscopy) I Projection and arrangements of neurons in the lamina ganglionaris of Diptera. *Zeitschrift der Zellforschung.* 121:377–441.

Strausfeld, N. J. 1976. Atlas of an Insect Brain. First edition. Springer-Verlag, Berlin Heidelberg. 215 pp.

Uusitalo, R. O., and M. Weckström. 1994. The regulation of chloride homeostasis in the small non-spiking visual interneurons of the fly compound eye. *Journal of Neurophysiology.* 71:1381–1389.

van Hateren, J. H. 1986. Electrical coupling of neuro-ommatidial photoreceptor cells in the blowfly. *Journal of Comparative Physiology A.* 158:795–811.

van Hateren, J. H. 1992*a*. Real and optimal neural images in early vision. *Nature.* 360:68–70.

van Hateren, J. H. 1992*b*. Theoretical predictions of spatiotemporal receptive fields of fly LMCs, and experimental validation. *Journal of Comparative Physiology A.* 171:157–170.

van Hateren, J. H. 1992*c*. A theory of maximizing sensory information. *Biological Cybernetics.* 68:23–29.

van Hateren, J. H. 1993. Spatiotemporal contrast sensitivity of early vision. *Vision Research.* 33:257–267.

Weckström, M., E. Kouvalainen, K. Djupsund, and M. Järvilehto. 1989. More than one type of conductance is activated during responses of blowfly monopolar neurones. *Journal of Experimental Biology.* 144:147–154.

Weckström, M., R. C. Hardie, and S. B. Laughlin. 1991. Voltage-activated potassium channels in blowfly photoreceptors and their role in light adaptation. *Journal of Physiology.* 440:635–657.

Weckström, M., M. Juusola, and S. B. Laughlin. 1992*a*. Presynaptic enhancement of signal transients in photoreceptor terminals in the compound eye. *Proceedings of the Royal Society of London B.* 250:83–89.

Weckström, M., E. Kouvalainen, and M. Juusola. 1992*b*. Measurement of cell impedance in frequency domain using discontinuous current clamp and white-noise-modulated current injection. *Pflügers Archiv.* 421:469–472.

Weckström, M., M. Järvilehto, and K. Heimonen. 1993. Spike-like potentials in the axons of non-spiking photoreceptors. *Journal of Neurophysiology.* 69:293–296.

Wong, F. 1978. Nature of light-conductance changes in ventral photoreceptors of Limulus. *Nature.* 276:76–79.

Wong, F., B. W. Knight, and F. A. Dodge. 1982. Adapting bump model for ventral photoreceptors of *Limulus*. *Journal of General Physiology.* 79:1089–1113.

Zettler, F., and M. Järvilehto. 1971. Decrement-free conduction of graded potentials along the axon of a monopolar neuron. *Zeitschrift der vergleichende Physiologie.* 75:402–421.

Zettler, F., and M. Järvilehto. 1972. Lateral inhibition in an insect eye. *Zeitschrift der Vergleichende Physiologie.* 76:233–244.

Zettler, F., and H. Straka. 1987. Synaptic chloride channels generating hyperpolarizing responses in monopolar neurones of the blowfly visual system. *Journal of Experimental Biology.* 131:435–438.